Journal of Materials Science: Materials in Engineering

ORIGINAL PAPER

Open Access

Three new reduced forms of synthesized Schiff bases as potent anti-corrosion inhibitors for carbon steel in artificial seawater

Hojat Jafari[1*], Elham Ameri[1], Fariba Soltanolkottabi[1] and Avni Berisha[2]

Abstract

As part of the development of a new organic entity, we synthesized three new reduced forms of Schiff bases named 2,2′-(((2,2-dimethylpropane-1,3-diyl)bis(azanediyl)bis(methylene)disphenol (I1), 4,4′-(((2,2-dimethylpropane-1,3-diyl) bis (azanediyl)bis(methylene)bis(2-methoxyphenol) (I2), and 6,6′-(((2,2-dimethylpropane-1,3-diyl) bis(azanediyl) bis(methylene)bis(2-methoxyphenol) (I3). In order to develop new organic ligands to inhibit steel corrosion in 1M HCl solution, various electrochemical methods, such as electrochemical impedance spectroscopy (EIS) and potentiodynamic polarization (PDP), along with surface visualization through atomic force microscopy (AFM), were employed. PDP results revealed excellent inhibition by compound I3 (71%) at a concentration of 1 mg/L. These findings were supported by the observation of a protective layer formation during prolonged immersion of steel in a corrosive solution, with or without inhibitors. In addition to gaining insights into the interaction mechanism and adsorption mode, density functional theory, Monte Carlo, and molecular dynamic simulations were conducted, revealing valuable information about the interaction of the inhibitors with the steel surface. Average surface roughness (R_a) values obtained for the artificial seawater in the absence and presence of inhibitor are 887 nm for blank, 195 nm for I1, 158 nm for I2, and 105 nm for I3.

Keywords Reduced Schiff base, Seawater, Inhibition, Reaction number, Electrochemical measurement, Quantum chemical calculations

Introduction

Carbon steel degradation is one of the important phenomena that is observed in all domestic and industrial sectors (Jafari et al. 2024a, 2024b). Material loss and economic loss are the direct consequence of it. It mainly occurs due to chemical, electrochemical, or biochemical interactions unintentionally causing corrosion (Mohsenifar et al. 2016; Jafari and Sayin 2016a, 2016b). Carbon steel used in industry is expected to have certain properties, the most important of which is corrosion resistance. Despite having the best corrosion resistance, commercial iron has poor machinability and weldability (Jafari and Sayin 2015a). The properties can be improved by alloying. Cu, Mn, Mg, Si, and other alloying elements are commonly used to give iron desirable properties (Ameri et al. 2022; Jafari and Akbarzade 2017; Jafari et al. 2013a). The API 5L series is the most popular engineering alloy group, with Mg and Si added as alloying elements. These are widely used in aerospace, aviation, defense, and other industries (Jafari et al. 2013a). The presence of alloying elements in them makes the API 5L have realistically good corrosion resistance properties. Pickling with hydrochloric acid, on the other hand, results in corrosion (Jafari et al. 2014). Pickling is usually carried out to remove the scales and rust formed on the surface of the

*Correspondence:
Hojat Jafari
hojatjafari80@yahoo.com
[1] Department of Chemical Engineering, Shahreza Branch, Islamic Azad University, P.O. Box 311-86145, Shahreza, Iran
[2] Department of Chemistry, Faculty of Natural and Mathematics Science, University of Prishtina, 10000 Prishtina, Kosovo

material. During this process, the metal may undergo disintegration. API 5L grade B has a wide range of applications in defense, aviation, industries, construction, and domestic means (Mohsenifar et al. 2016; Jafari and Sayin 2016a). As a result, corrosion control on API 5L carbon steel must be addressed. In addition to these characteristics, API 5L carbon steels are prone to corrosion in a chloride ion-containing medium. This leads to the destruction of the material. Therefore, it is necessary to control corrosion. One of the methods to control the corrosion rate is to add inhibitors to the corrosive media. Due to the presence of the –C=N– group, an electron cloud on the aromatic ring, the electronegative N, O, and S atoms in the molecule, Schiff bases may be good corrosion inhibitors (Jafari et al. 2013b). Schiff bases have been previously reported as effective corrosion inhibitors for steel in acid mediums like hydrochloric acid. Schiff bases inhibit corrosion better than Amides and Aldehydes, which reduce the corrosion rate (Benmahammed et al. 2019). The inhibition efficiency of Schiff base compounds will increase by adding halogens to their composition due to the increase in electron density (Zhang et al. 2012, 2018; Saha et al. 2015). N_2O_2, $-NO_2$, $-CH_3$, and $-Br^-$ are various substitutes in structers of Schiff bases which are the most effective because of their higher electron donation ability. The presence of these substitutes will improve the substrate's physical connection and inhibition and efficiency (Jafari et al. 2024a, 2013b; Negm et al. 2011; Jafari and Ameri 2024). NO group in Schiff base compounds has various applications in catalyst industries because of their particular surface properties (Jafari and Akbarzade 2017; Jafari et al. 2014, 2013b; Jafari and Sayin 2015b). Dinitrogen tetroxide Schiff bases also protect steel against corrosion in H_2SO_4 media (Rezaeivala et al. 2022). In addition, these compounds inhibit corrosion on the steel surface against corrosive ions, especially in acidic solutions. By comparing the examined Schiff base with other inhibitors of steel in acidic media that have been reported, the comparison makes it evident that the compound we evaluated had high corrosion efficiency in the HCl environment.

In this work, the reduced Schiff bases form compounds have the formula2,2'-(((2,2-dimethylpropane-1,3-diyl)bis(azanediyl)bis(methylene)disphenol (I1), 4,4'-(((2,2-dimethylpropane-1,3-diyl)bis(azanediyl)bis(methylene)bis(2-methoxyphenol) (I2), and 6,6'-(((2,2-dimethylpropane-1,3-diyl)bis(azanediyl)bis(methylene)bis(2-methoxyphenol) (I3) were investigated for the first time by Tafel, Electrochemical Impedance Spectroscopy (EIS), and AFM tests in the artificial seawater. The solutions containing concentrations of 1 mg/L of three inhibitors were used, and the effects of electronic structure and chemical structure of derivatives on inhibition efficiency and comparison of the effect of different substituents were evaluated. Quantum and molecular simulation methods have also been performed as part of this work.

Experimental procedure

The electrodes were prepared from API 5L B carbon steel specimens. The specimens of dimension 1 cm × 1 cm (exposed) (isolated with polyester resin) were used for polarization and electrochemical impedance methods. They were polished mechanically using different grade emery papers from 220 up to 2000 and washed thoroughly with triple distilled water and degreased with acetone before being immersed in the acid solution.

The testing solution was artificial seawater with 3% concentrations of Cl – (wt.%). The artificial seawater was prepared with ultra-pure water and A.R. reagents including NaCl, $MgCl_2$, and $CaCl_2$.

Three synthesized Schiff base named 2,2'-(((2,2-dimethylpropane-1,3-diyl)bis(azanediyl)bis(methylene)disphenol (I1), 4,4'-(((2,2-dimethylpropane-1,3-diyl)bis(azanediyl) bis(methylene)bis(2-methoxyphenol) (I2), and 6,6'-(((2,2-dimethylpropane-1,3-diyl)bis(azanediyl)bis(methylene) bis(2-methoxyphenol) (I3) was prepared according to the described procedure (Benmahammed et al. 2019; Keypour et al. 2008, 2009, 2013). For I1, 2,2-dimethylpropane-1,3-diamine (0.20 g, 2 mmol) and salicylaldehyde (0.48 g, 4 mmol) were mixed in methanol (30 ml). The stirred mixture was refluxed for 6 h. The solution was filtered, and the filtrate volume was reduced to ca. 10 ml. The obtained compound was washed with methanol and dried in a desiccator. For I2, 2,2-dimethylpropane-1,3-diamine (0.20 g, 2 mmol) and 2-hydroxy-3-methoxybenzaldehyde (0.60 g, 4 mmol) were mixed in methanol (30 ml). The stirred mixture was refluxed for 6 h. The solution was filtered, and the filtrate volume was reduced to ca. 10 ml. The obtained compound was washed with ethanol and dried in a desiccator. For I3, 2,2-dimethylpropane-1,3-diamine (0.20 g, 2 mmol) and 4-hydroxy-3-methoxybenzaldehyde (0.60 g, 4 mmol) were mixed in ethanol (30 ml). The stirred mixture was refluxed for 2 h. The solution was filtered, and the filtrate volume was reduced to ca. 10 ml. The obtained compound was washed with ethanol and dried in vacuo.

The concentration of inhibitors employed was 1 mg/L. Figure 1 shows the Schiff base ligands of this study.

Atolab device was used to perform polarization tests. The tests were performed on a standard cell containing platinum wire as an auxiliary electrode and calomel as a reference electrode. The experiments were performed at room temperature. At the beginning of each experiment, an interval of about 30 min was applied to stabilize the potential of the components in the solution from the potential range of about – 500 to 100 mV compared to the open circuit potential and scan rate of 1 mV/s.

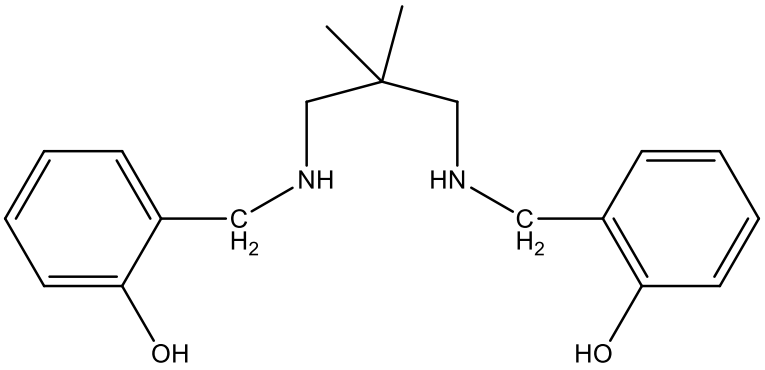

Molecular Weight: 314.4219

I1

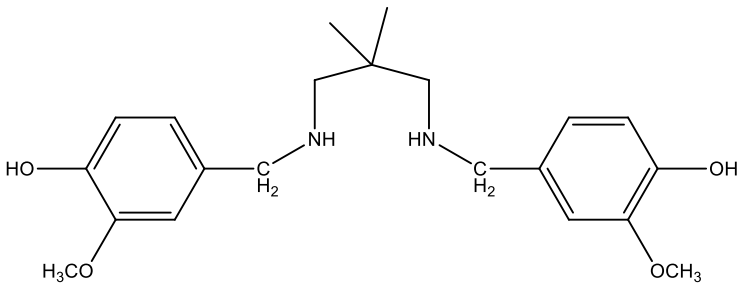

Molecular Weight: 374.4739

I2

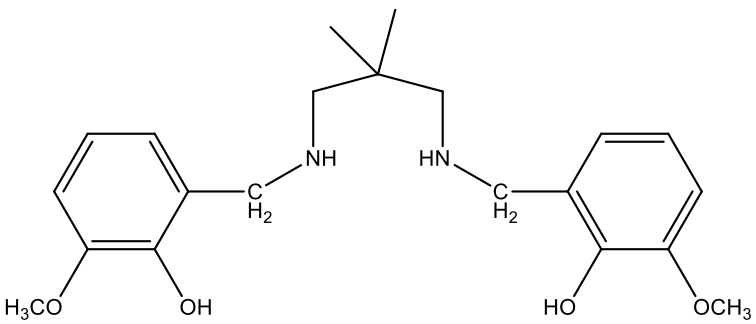

Molecular Weight: 374.4739

I3

Fig. 1 The chemical structure of the inhibitors

An electrochemical test was performed for steel samples after 30 min of immersion in the solutions. For this purpose, a three-electrode electrochemical cell including counter electrode (graphite), reference electrode (calomel electrode), and working electrode (steel sample) is connected to a computer-controlled

AutoLab potentiostat/galvanostat system (PGSTAT 302) and tested in open circuit potential in the frequency range of 100 kHz to 10 MHz with a peak amplitude of 10 mV A.C.

The Frontier molecular orbitals (FMOs) were studied using the Materials Studio software program's DMol3 module (Oyeneyin et al. 2022; Quraishi et al. 2009; Timoudan et al. 2024; Zaroual et al. 2024). The dual scalar and polarization basis set (DNP) (Zhao and Truhlar 2008; Furtado et al. 2022) in combination with functional M06-L (M. Ben Hadj Ayed, T. Osmani, N. Issaoui, A. Berisha, B. Oujia, H. Ghalla 2019; Mardirossian and Head-Gordon 2017; Klamt 2005) was utilized to improve the geometrical features of all inhibitors in order to have a better understanding of the electronic correlation between them. In order for the field to converge in a self-consistent approach, there has to be a difference in energy of less than 10^{-7} Ha. For the purpose of including the solvent, water, in the density functional theory (DFT) computations, the conductor-like screening model (COSMO) was utilized (Klamt 2018; Berisha 2019a; Faydy et al. 2021).

To study the plausibility of interactions between the inhibitor molecules and the iron (110) surface atoms, the Adsorption Locator tool in Material Studio was utilized in conjunction with Molecular and Molecular Dynamics software. A cell with the dimensions 2.482 nm × 2.482 nm × 1.32 nm, in which a vacuum slab extends 3.5 nm on top of the cell's Fe(110) surface.

The MC simulations were carried out by continually loading one inhibitor molecule (I1, I2, or I3) into a simulated cell, along with corrosive species such the following: H_2O (800), Na^+ (5), Ca^{2+} (2), Mg^{2+} (2), and Cl^- (13) and simulating the effects of these corrosive species using the Adsorption locator module in Material Studio. Because it was believed that this layer would include reasonable sites for the inhibitor molecule to adsorb, the target atoms for the MC simulation were specifically selected from the very top layer of the Fe(110) slab. As a direct result of drawing the conclusion of the simulation, the equilibrium adsorption configuration that required the least amount of energy to maintain was investigated and characterized. The subsequent phase in our process was making use of the well-known COMPASS forcefield and running MD simulations in the Forcite module of Material Studio at a temperature of 298 K with all of the Fe(110) atoms, with the exception of the top two layers, frozen (with a time step of 1.0 fs). The simulation acquired 2 ns (Dagdag et al. 2021a; Jafari et al. 2022a). Using the trajectory of the MD simulation, a radial distribution function, or RDF, was made in order to make a classification of how the inhibitor molecule binds.

The solubility test of the prepared Schiff base ligand was determined in different solvents such as distilled water, ethanol, methanol, dimethylsulfoxide, dimethylformamide, acetone, and acetic acid by shaking a small amount of each of the compounds in a test tube containing 10 ml portions of each of the solvents.

The solubility of the Schiff base ligands was determined in different solvents. From the result of the solubility test, it can be observed that the ligands were soluble in hydrochloric acid, dimethylsulfoxide, and dimethylformamide; slightly soluble in ethanol and methanol; and insoluble in water and soluble in acetone.

The steel samples were exposed to 1 mgL^{-1} of these compounds in the artificial seawater for 7 days of immersion at ambient temperature. Then, the changes that occurred on the surface were evaluated by atomic force microscope (AFM) NanoSurf easyscan2.

Results

Open-circuit potential (OCP)

The potential created between seawater and the samples, which is the steel surface under study, in relation to a SCE electrode that will be put into the solution near the working electrode, is known as the open circuit potential. The collected results showed that before the impedance and polarization experiments started, the solutions under investigation had acquired a satisfactory level of stability. The OCP value first varied for blank before stabilizing. However, when the samples were added to 1 mg/L of three ligands, I1, I2, and I3, there was a discernible fluctuation that shifted in a negative direction throughout the course of the time. The value of OCP remained stable and was trending upward. Three ligands, I1, I2, and I3, had steady and unstable adsorption on the steel sample's surface. It could be the cause of behavioral abnormalities (Fig. 2).

Potentiodynamic polarization results

To understand the interactions between inhibitor ligands and steel in an acidic solution, the PDP study was performed at different concentrations of I1, I2, and I3. Figure 2 shows the PDP curves for carbon steel without and with the addition of I1, I2, and I3 molecules in the corrosive medium at a temperature of 25℃ for 3 days. The electrochemical settings are summarized in Table 1.

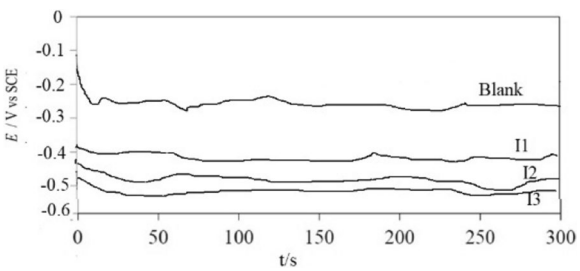

Fig. 2 OCP curve

Table 1 Potentiodynamic polarization measurements for steel in water for 3 days

	$b_a(mV) \pm 1$	$b_c(mV) \pm 1$	$i_{corr}\ (\mu Acm^{-2}) \pm 10^{-2}$	$R_p(\Omega Cm^{-2}) \pm 10^{-2}$	$-E_{corr}(V) \pm 1$	$\theta \pm 10^{-2}$
I3	28	−120	2.132	7.55	235	0.71
I2	36	−199	3.058	6.51	239	0.58
I1	44	−209	3.698	6.20	253	0.49
Blank	37	−163	7.336	2.86	273	–-

Examination of the electrochemical parameters related to the graphs in Fig. 3 reveals that the addition of organic molecules I is reflected by a displacement of the current intensity towards lower values compared to the value calculated in the control, and an efficiency more marked inhibitor. Furthermore, it is clearly observed that the addition of three ligands, I1, I2, and I3, in a corrosive environment shifts the corrosion potential towards more cathodic values compared to the control. This results in a reduction in anodic and cathodic current densities, thus slowing down the metal dissolution in the acidic solution (Dagdag et al. 2021a; Rahimi et al. 2022). Apparently, the incorporation of I1, I2, and I3 ligands in the acidic solution induces significant changes in the slopes of the anodic and cathodic Tafel curves, suggesting alterations in reaction mechanisms. However, unlike the cathodic behavior, the slope of the anodic Tafel curve decreases compared to the inhibitor-free environment, indicating that the organic molecules of I ligands significantly slow down the rate of metal degradation by modifying the anodic reaction mechanism (Bhardwaj et al. 2022). Similarly, the results in Table 1 indicate that the addition of these ligands in the corrosive environment has no significant effect on the anodic and cathodic slope values. The cathodic Tafel curves remain largely parallel in inhibited and uninhibited solutions. This reflects the remarkable influence of the ligands on inhibiting the hydrogen evolution reaction rate without altering the mechanism of this reaction through a simple blocking effect, making it difficult for H^+ ions to reach the metal surface and undergo reduction (Ganjoo et al. 2022; Daoudi et al. 2022; Ouass et al. 2021a). Consequently, the reduction of H^+ ions can only occur on the unprotected metal surface or if H^+ ions reach the carbon steel surface through the partially blocked pores of the inhibitor film, which occurs through a charge transfer mechanism (Damej et al. 1254). On the other hand, Fig. 2 clearly shows that I1, I2, and I3 act as a mixed-type corrosion inhibitor. As a result, it can be stated that these ligands reduce both the H^+ ion reduction reaction and the iron degradation reaction (Ould Abdelwedoud et al. 2022; Mehmeti 2022). However, the inhibitory effectiveness of the three synthesized organic compounds decreases in the order I3 > I2 > I1, with an excellent inhibitory efficiency reaching 71% for I3. This ranking can be attributed to the structure of the inhibitors, including the presence of functional groups, substitution groups, the number of heteroatoms, and π electrons. The presence of the methoxy ($-OCH_3$) and hydroxyl ($-OH$) groups enhances the protection provided by these ligands. Therefore, the adsorption of I3 on the steel surface is more pronounced compared to other ligand, which has a flat structure.

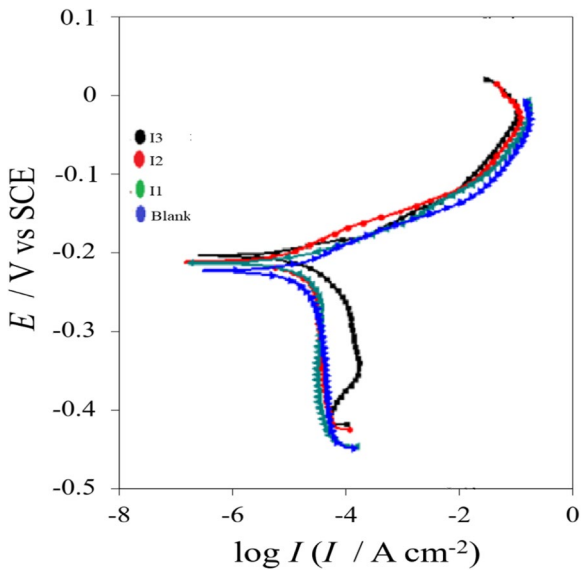

Fig. 3 Potentiodynamic plots for corrosion of steel (with and without inhibitors) in Demineralised water

This suggests that a change in compound does not change the steps involved in the anodic and cathodic reactions. There is $a + 2$ to $+4$ mV change in corrosion potential with adding inhibitors for steel in water. With the introduction of coating, the maximum displacement of lower than -38 mV in corrosion potential was observed. These insights that the blocking effect of compounds and its filler is more at the cathode compared to the anode. The corrosion inhibition efficiencies of the ligands were reduced in the following order: I3 > I1 ≈ I2.

Electrochemical impedance spectroscopy

Figure 3 represents Bode and Nyquist plots. Nyquist plot obtained by taking an imaginary part of impedance on the *Y*-axis and the real part of impedance on

the *X*-axis for the corrosion of steel with and without coating.

As observed from Fig. 4, the shape of the curves is half-circle, which implies that the transfer of charges takes place between steel and water.

The semi-circles were diminished, this may be due to non-homogeneity on the metal surface causing the variation in frequency. The non-homogeneity may be due to the deposition of ferric oxide or other ions on the steel surface. The semi-circle diameter represents the resistance to the exchange of ions at the mild steel-fresh/demineralized water interface (R_{ct}). With adding the inhibitors, the diameter of semicircles increases, this observation may be due to the decrease in the mobility of ions of water and reactivity of the steel surface.

With additional inhibitors, C.E. increased that shows an increase in the adsorbing tendency of the compounds does not efficiently increase the charge transfer at the metal solution interface, or decreased charges at the double layer due to an increase in viscosity of the medium, or the number of reactive sites is decreased due to decrease in conductivity of steel. Due to the combined effect of all or any one to two effects may be dominating with adding inhibitors.

The Nyquist plots are evaluated by applying the impedance Excel data to the Zimpfin software to get the

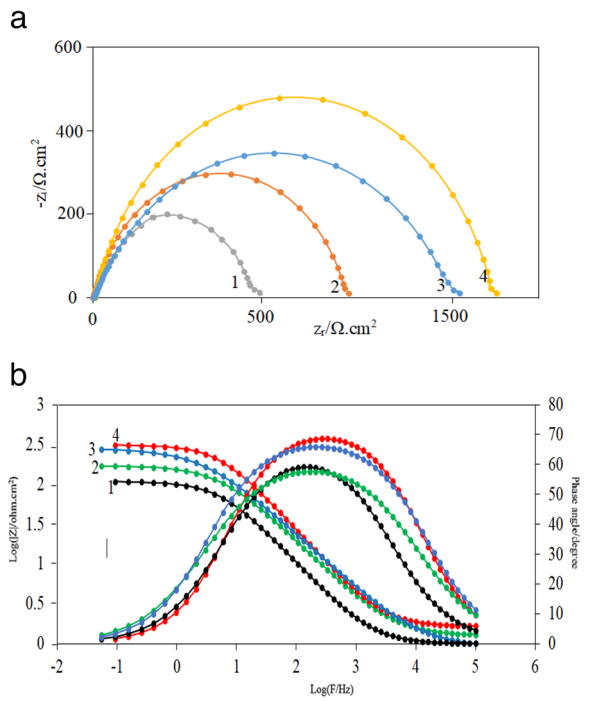

Fig. 4 **a**. Nyquist plot for corrosion of steel in water: (1) blank, (2) I1, (3) I2, (4) I3. **b**. Bode plot for corrosion of steel in water: (1) blank, (2) I1, (3) I2, (4) I3

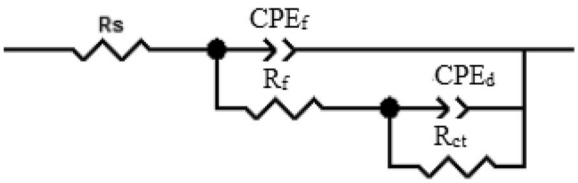

Fig. 5 Equivalent circuit for impedance data fitted for steel in water

appropriate equivalent circuits. The satisfactory equivalent circuit is shown in Fig. 5.

R_s is the resistance offered by the solution present between anode and cathode, constant phase element 1 (*CPE* 1), the electrical double layer dielectric constant, *CPE* 2 capacitance of the passive ferric oxide film, and R_f film resistance. Due to the irregular surface, the charged layer present on the steel surface and water boundary is not a perfect capacitor. Hence, it is replaced by CPE (Fakhry et al. 2024; Alamiery et al. 2021).

The CPE impedance is calculated using Eq. (1):

$$Z = Q^{-1}(\mathrm{iw})^{-n} \tag{1}$$

The Q is the proportionality coefficient; $w = 2\,\pi\mathrm{fmax}$ is the angular frequency; fmax is the frequency at which the imaginary component of the impedance is maximum, i is the imaginary number, and the power n is associated with the phase shift. If $n = 1$, then the charged double layer at the boundary behaves like an ideal capacitor. The correction in the capacitance to its real value is calculated using Eq. (2).

$$C_{\mathrm{dl}} = Q(w)^{n-1} \tag{2}$$

The C_{dl} at the steel water with and without coatings was evaluated using (3).

$$C_{\mathrm{dl}} = 1/2\pi\,\mathrm{fmax}.R_p \tag{3}$$

The polarization resistance R_p at the steel water with and without coatings was calculated using (4).

$$R_p = R_{\mathrm{ct}} + R_f + R_s \tag{4}$$

From Table 2 and Fig. 3, it is observed that R_s with and without inhibitors in water have the nearly same value. By introducing inhibitors on steel R_p value rises, and C_{dl} values suppress. It confirms the blocking of active centers present on steel surfaces by the molecules of Schiff bases. The inhibition effect of compounds was enhanced by adding I3. At the steel surface and water interface net exchange of charges decreases (resistance to charge transfer R_{ct} increases) and the thickness of the electrical double layer increases due to the presence of inhibitors of big Schiff-base molecules. Therefore, by introducing inhibitors, capacitance rises, and resistance to shifting

Table 2 Impedance data for steel in water for 3 days

	R_{s} / Ω cm^2 ± 10^{-3}	CPE1-T/ μF cm^{-2} ± 10^{-2}	CPE1-P/ μF cm^{-2} ± 10^{-3}	R_{1} / Ω cm^2 ± 10^{-3}	CPE2-T/ μF cm^{-2} ± 10^{-2}	CPE2-P/ μF cm^{-2} ± 10^{-3}	R_{2}/ Ω cm^2 ± 1	$\theta \pm 10^{-2}$	$\chi^2 \pm 10^{-3}$
I3	3.197	5.30	0.875	2.893	188.57	0.694	1792	0.72	0.017
I2	2.724	3.41	0.807	2.561	214.44	0.703	1289	0.60	0.015
I1	2.464	5.97	0.804	2.141	318.51	0.665	780	0.38	0.018
Blank	2.345	3.24	0.842	4.235	136.22	0.718	486		0.018

equilibrium potential from the net corrosion current (R_p) rises at the steel and water interface increases.

Density functional theory

In the preliminary step of the approach, a conformer search (Faydy et al. 2023; Akkermans et al. 2020) was performed utilizing the Boltzmann jump search method, using 2000 as the number of searched conformer structures and the COMPASS III forcefield (Molhi et al. 2021a). This was done in order to acquire the lowest feasible start energy for the molecule while also quickening the density functional theory (DFT) computations. DFT calculations began by picking the conformer with the lowest energy level, as illustrated in Fig. 6.

The sigma-profile charge density curve is created using calculations based on the COSMO model. The electrostatic potential in COSMO is represented by the use of partly charged atomic nuclei (Faydy et al. 2021; Berisha 2019b; Rahimi et al. 2022). Figure 7 is an illustration that depicts how an inhibitor can perform either the role of an acceptor or a donor of H-bonds.

H-bond acceptor/donor interactions between water molecules occur when an inhibitor is dissolved in water. This property controls how soluble the inhibitor is (Bhardwaj et al. 2022; Ganjoo et al. 2022).

As seen in Fig. 8, HOMO in the inhibitor molecules is positioned on one side of the ring containing O atoms, whereas LUMO is located on the opposite side of the ring, implying that these parts of the molecule can are prone to electron transfer to/from the metal's surface (Daoudi et al. 2022; Ouass et al. 2021a; Damej et al. 1254).

This exchange of electrons consequently results in the generation of a protective organic layer that coats

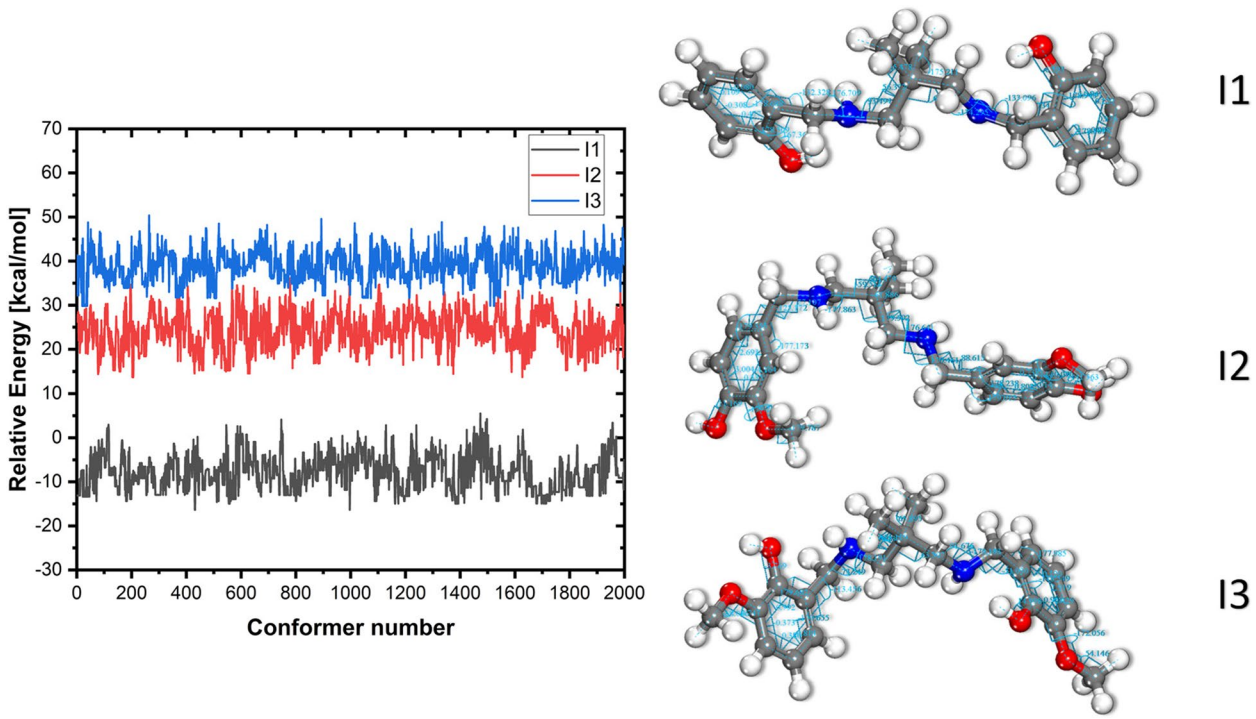

Fig. 6 The conformer search's energy profile and the inhibitors' corresponding lowest energy structures

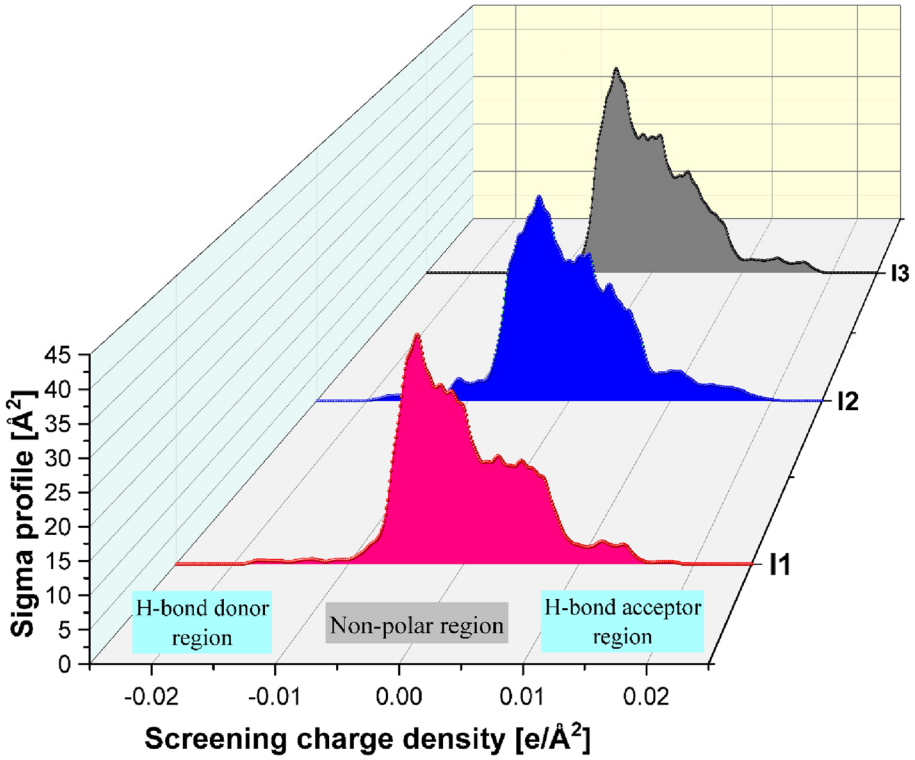

Fig. 7 COSMO profiles of the inhibitors

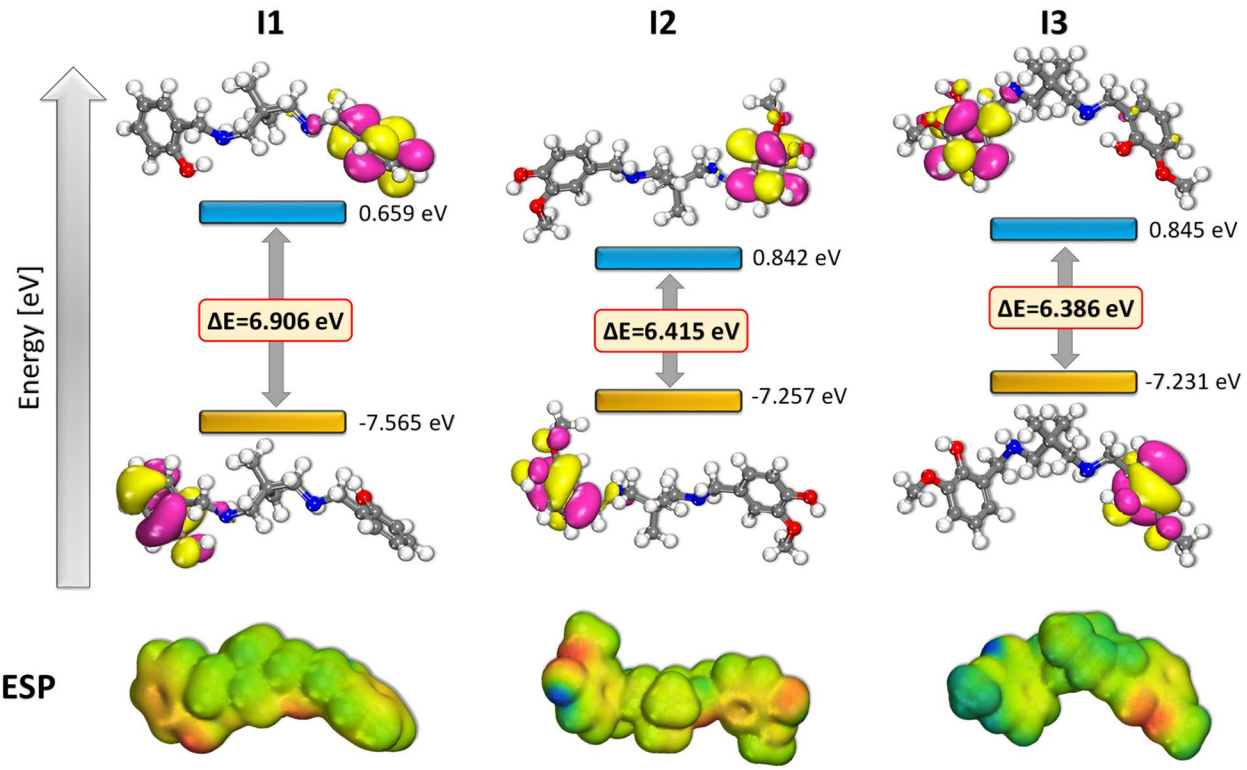

Fig. 8 HOMO, LUMO and ESP of the inhibitors

the surface of the metal and preserves it from corrosion (Akkermans et al. 2020; Bhardwaj et al. 2022; Ganjoo et al. 2022; Ould Abdelwedoud et al. 2022; Mehmeti 2022). Electron acceptors, also called LUMOs, are parts of an inhibitor's structure that are responsible for taking electrons from a surface with a lot of electron density, like the surface of a metal (Bhardwaj et al. 2022; Daoudi et al. 2022; Ouass et al. 2021a). As a result of the exchange of lone pair electrons between heteroatoms (N and O) and the vacant iron d-orbital, which consequences in a moderate rise in surface absorption potential, it is presumed that adsorption on the surface of the metal will be significantly greater. This is because the exchange of lone pair electrons results in a moderate rise in surface absorption potential (Bhardwaj et al. 2022; Mehmeti 2022; Jafari et al. 2022b).

Table 3 contains the most regularly used descriptors, which are organized by frequency of usage (the equations used to calculate them can be found in the following references) (Damej et al. 1254; B. Ould abdelwedoud, M. Damej, K. Tassaoui, Berisha, H. Tachallait, K. Bougrin, V. Mehmeti, M. Benmessaoud 2022; Dagdag et al. 2021b). DFT simulations of inhibitor adsorption can help understand inhibitor adsorption mechanisms. Numerous studies suggest that the inhibitors' ability to exchange electrons with Fe(110) supports its adsorption. The inhibitors' low electron affinity and large ionization potential sustenance this interpretation (Table 3). Chemical softness and hardness predict the inhibitor's metal-surface adsorption affinity (Dagdag et al. 2021a; Berisha 2021; Kalai et al. 1191).

High values of chemical softness are also expected to show the inhibitor's affinity for the metal surface. Inhibitors have an ΔE value in the range of − 1, which reflects their aptitude to receive electrons from the Fe(110) surface.

The Mulliken atomic charges (MAC) are a key factor in determining which atoms, typically known as inhibitory sites, are involved in the process of metal adsorption (Bhardwaj et al. 2022; Mehmeti 2022; Molhi et al. 2021b).

Numerous studies have shown that it is more probable for Fe(111) O surface atoms and inhibitor molecules to interact when the inhibitor atoms have a negative atomic charge (MAC). This has been shown both experimentally and theoretically. The MAC values of the inhibitors are displayed in Fig. 9, and these are the atoms that we are interested in. The atoms of oxygen and nitrogen in the inhibitors have significant negative charges, which indicates that these centers contain the greatest electron density and are thus able to adhere to metal surfaces with the greatest degree of success. Figure 7 presents the molecular electrostatic potential, also known as MEP, of the inhibitors at varying concentrations (area in red) (Jafari et al. 2022a; Berisha 2019b; Haldhar et al. 2021; Guo et al. 2014).

Monte Carlo and molecular dynamic simulations

Throughout this case, the adsorption energy may be easily calculated by beginning with the Fe(110) surface. Adsorption energy may be calculated using the following equation: (Eads) (Berisha 2021; Hsissou et al. 2019;

Table 3 Calculated theoretical chemical parameters for the inhibitors

Descriptor	I1	I2	I3
HOMO	− 7.5650	− 7.2570	− 7.2310
LUMO	0.6590	0.8420	0.8450
ΔE(HOMO–LUMO)	6.906	6.415	6.386
Ionization energy (I)	7.5650	7.2570	7.2310
Electron affinity A)	− 0.6590	− 0.8420	− 0.8450
Electronegativity (X)	3.4530	3.2075	3.1930
Global hardness (η)	4.1120	4.0495	4.0380
Chemical potential (π)	− 3.4530	− 3.2075	− 3.1930
Global softness (σ)	0.2432	0.2469	0.2476
Global electrophilicity (ω)	1.4498	1.2703	1.2624
Electrodonating (ω −) power	3.6903	3.3802	3.3637
Electroappcepting (ω +) power	0.2373	0.1727	0.1707
Net electrophilicity (Δω + -)	0.0337	0.1231	0.1266
Fraction of transferred electrons (ΔN)	− 0.0271	0.0028	0.0046
Energy from Inhb to Metals (ΔN)	0.0030	0.0000	0.0001
ΔE back donation	− 1.0280	− 1.0124	− 1.0095

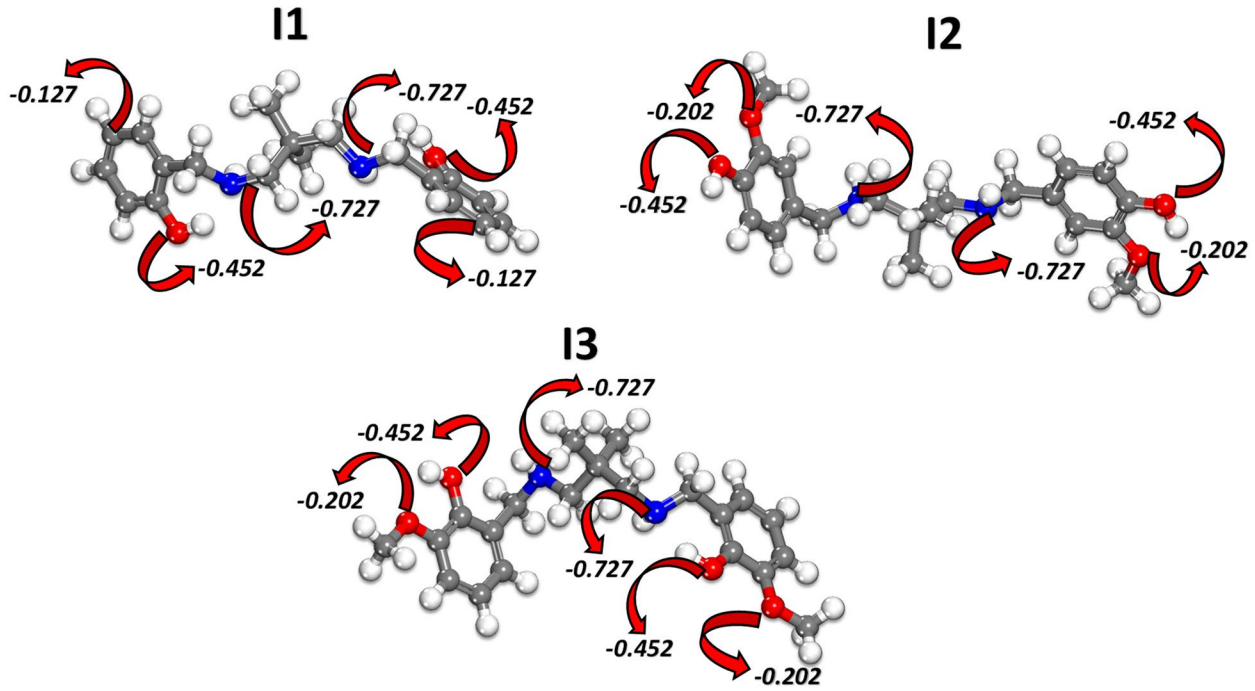

Fig. 9 Mulliken atomic charge (MAC) values for heteroatoms in the selected inhibitor atoms

Dagdag et al. 2019, 2020; Hsissou et al. 2019; Abbout et al. 2020):

$$E_{\text{adsorption}} = E_{\text{Fe(110)}_{||}\text{inhibitor}} - \left(\text{Fe}_{(110)} + E_{\text{inhibitor}}\right) \quad (5)$$

where $E_{\text{Fe(110)}_{||}\text{inhibitor}}$ is the total energy of the simulated system, $E_{\text{Fe,}}$ and $E_{\text{inhibitor}}$ is the total energy of the Fe(110) surface and the corresponding free inhibitor molecules.

As a last step in verifying the accuracy of the MC calculations, the inhibitor's adsorption geometry was examined in detail. Checking whether equilibrium can be reached in the MC simulation using the steady-state energy levels. As the simulation progressed, the system eventually settled into its lowest-energy condition. Inhibitor arrangement on a possible Fe(110) plane is shown in Fig. 6. The backbone of an inhibitor molecule adhering to the surface atoms of the Fe(110) plane may be responsible for the observed adsorption pattern (directed by heteroatoms, mainly O) (Ouass et al. 2021b; Jessima et al. 2020).

Adsorption is caused when molecules exhibit their heteroatoms and electron rings at the surface, which is what gives them the capacity to absorb. Adsorption is what gives molecules their ability to absorb (Akkermans et al. 2020; Ganjoo et al. 2022). The adsorption of inhibitors results in the formation of massive E_{ads} (Fig. 10) on the surface of the metal. These inhibitor compounds have a significant adsorption interaction with the metal due to the exceptionally high adsorption energies that they possess. By making use of this contact, a protective layer may be formed, which serves to shield the metal surface from the effects of corrosion. Based on the E_{ads} values that were found through MC, the order of corrosion inhibition performance of the inhibitors is I3 > I1 ≈ I2. The MD model of adsorption dynamics is generally acknowledged to be the more accurate of the two (Dagdag et al. 2021a; Faydy et al. 2023; Akkermans et al. 2020; Berisha 2019b; Ouass et al. 2021a). After several hundreds of ps of NVT simulation, it is clear that the inhibitors in Fig. 10 adopt a horizontal structure on one side of the molecule rings onto the metal surface and are substantially adsorbed onto the Fe surface (Fig. 11).

Adsorption processes are generally portrayed on the RDF graph of metal surfaces if peaks form at a specific distance from the metal surface (Jessima et al. 2020). When the heights are in the zone of 1–3.5 Å in range, it is thought to indicate a chemisorbable process. On the other hand, for physical adsorption, RDF peaks are expected to be present at distances larger than 3.5 Å (Bhardwaj et al. 2022; Ganjoo et al. 2022; Daoudi et al. 2022; Ouass et al. 2021a; Damej et al. 1254).

Fe surface and inhibitor O and N atoms had RDF peak values at distances of less than 3.5 Å—except the I1

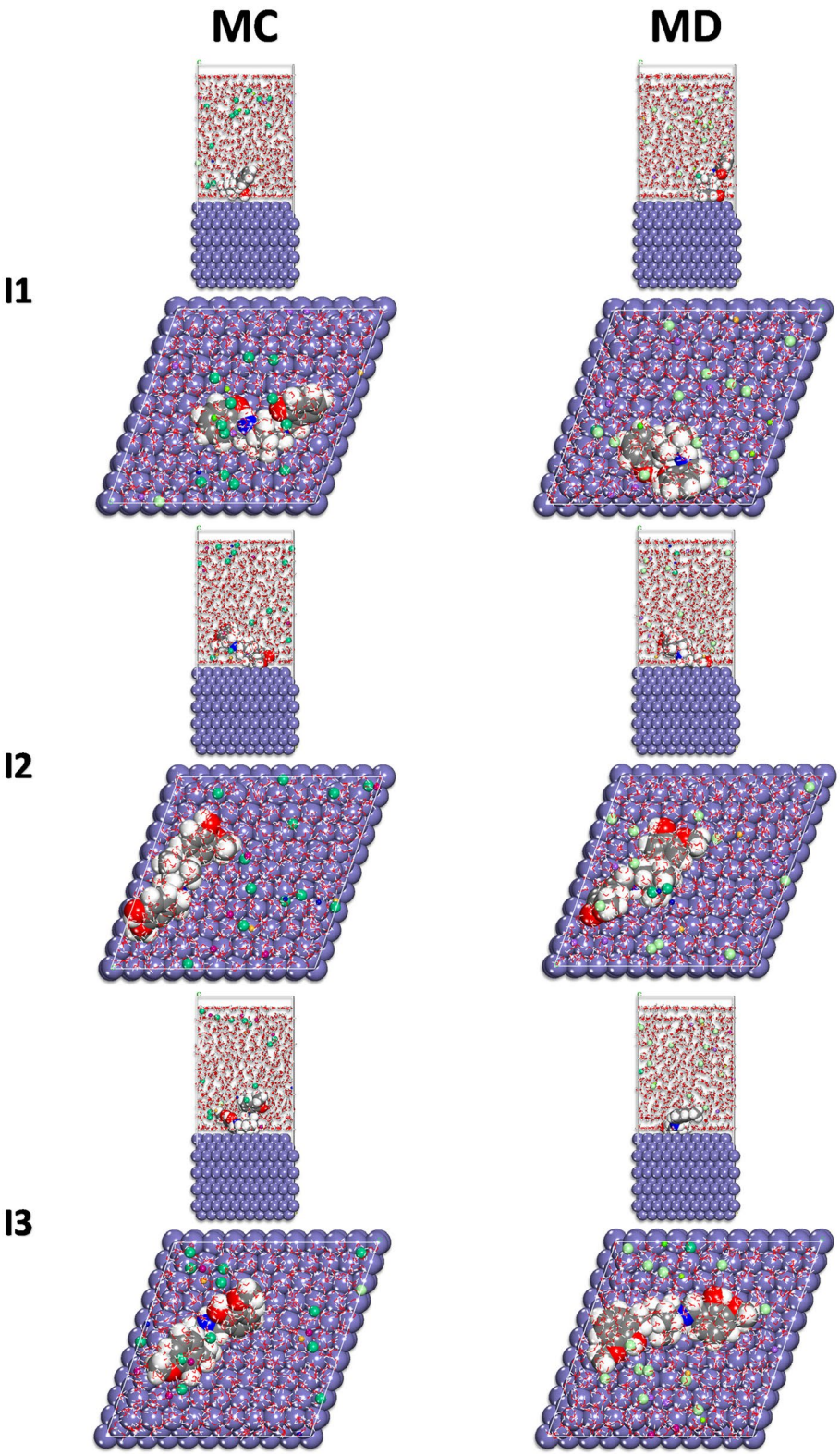

Fig. 10 The "image" of the examined inhibitor molecules on Fe(110) with the lowest energy, as calculated by MC and MD

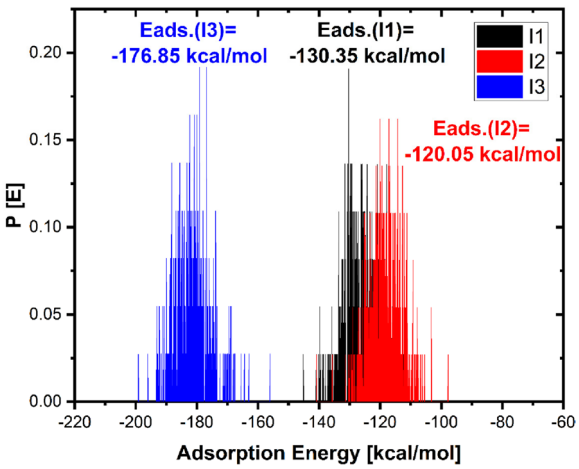

Fig. 11 Distribution of the adsorption energies for the inhibitors obtained via MC

molecule, where it seems that the N atoms have insignificant adsorption contribution to this molecule (Fig. 12) (Akkermans et al. 2020; Bhardwaj et al. 2022; Mehmeti 2022). As seen by its comparatively high negative energy value and RDF peaks, in this instance, the inhibitors seem to be significantly interacting with the surface of the metal through the O/N atoms.

Surface analysis

AFM has been widely utilized in the corrosion field to assess the 3D corrosion morphology of steel surfaces in recent research. The three-dimensional AFM images of polished steel surfaces, and specimens immersed in the artificial seawater with and without I1, I2, and I3, are shown in Fig. 13a, b, c, and d, respectively. The images obtained in the presence of I3 exhibited a smoother surface. Average surface roughness (R_a) values obtained for the artificial seawater in the absence and presence of inhibitor are 887 nm for blank, 195 nm for I1, 158 nm for I2, and 105 nm for I3. The decrease in the R_a values clearly demonstrates the adsorption of inhibitor molecules on the steel surface (Jafari and Sayin 2015b).

Conclusion

The inhibition efficiency of corrosion protection of API 5L B in seawater was increased with an increase in the addition of inhibitors. Three compounds have symmetrical two parts, and there are two benzene rings and two imine groups in each ligand. The adsorption of aromatic rings and heteroatom centers on the steel surface and the interaction of aliphatic moieties with the steel surface caused these compounds to have a good performance in protecting the steel against corrosion. The inhibiting effect of these compounds due to their adsorption operates via the formation of a barrier film on the metal surface. I3 has the best adsorption effect of these compounds; an important structural factor is a linear structure because it raises electrostatic interaction between Schiff bases and API 5L surface. Regarding this point, I3 is capable of forming a strong bond with the steel surface. Furthermore, electronegative O atoms helped the adsorption of this ligand on the steel surface. I1 and I2

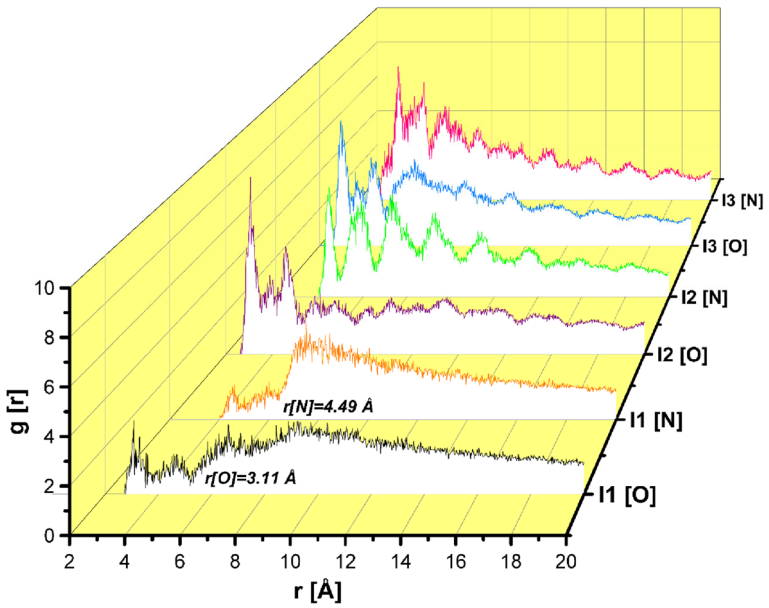

Fig. 12 The MD trajectory analysis was used to determine the RDF of heteroatoms (O and N) for the inhibitors that were adsorbed on the Fe (110) surface

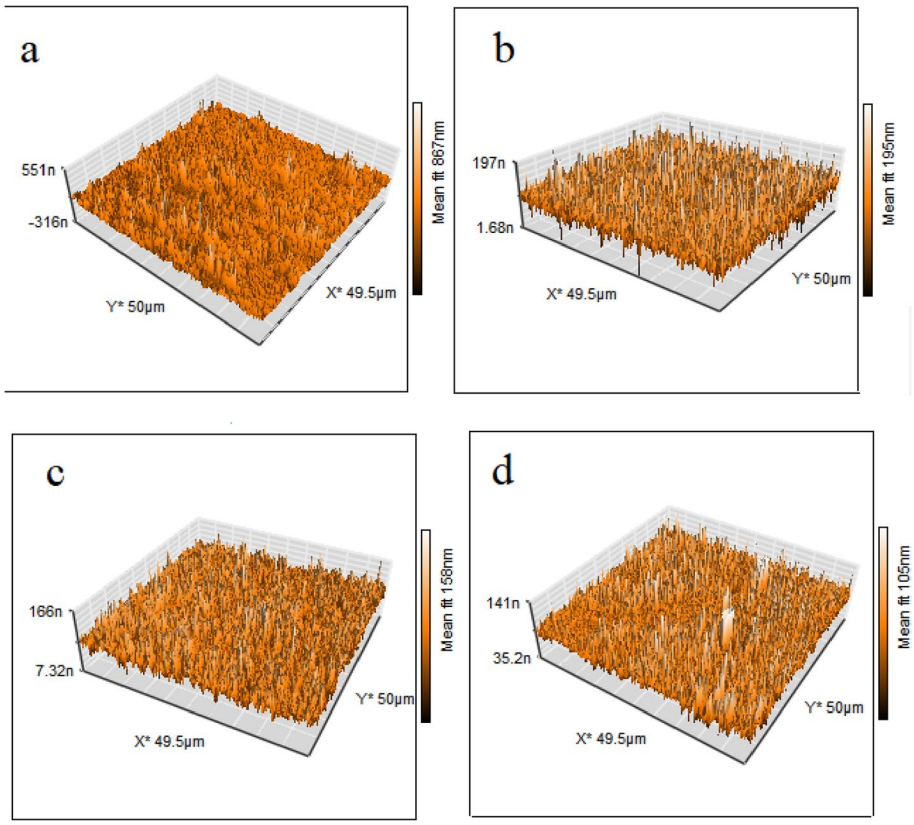

Fig. 13 Surface of steel electrode by AFM microscope at artificial seawater: (**a**) without, (**b**) with 1 mg/L I1 (**c**) with 1 mg/L I2 and (**d**) with 1 mg/L I3

are only different from the molecular structures of the substituents near the nitrogen atom. According to the results of the MD calculations, the inhibitor is mostly flat-adsorbed. The outcomes of the experiment provide the hypothesis that the inhibitor possesses large adsorption energies of the negative variety.

Authors' contributions

H. Jafari analyzed and interpreted the data. A. Berisha performed the experimental examination of the tests and was a major contributor to writing the manuscript. All authors read and approved the final manuscript.

Funding

The authors declare that no funds, grants, or other support were received during the preparation of this manuscript.

Availability of data and materials

The data that support the findings of this study are available from the corresponding author, upon reasonable request.

Declarations

Ethics approval and consent to participate

Not applicable.

Competing interests

The authors have no relevant financial or non-financial interests to disclose. On behalf of all authors, the corresponding author states that there is no conflict of interest.

Received: 7 June 2024 Accepted: 4 September 2024
Published online: 26 September 2024

References

Abbout S, Zouarhi M, Chebabe D, Damej M, Berisha A, Hajjaji N (2020) Galactomannan as a new bio-sourced corrosion inhibitor for iron in acidic media. Heliyon 6:e03574. https://doi.org/10.1016/j.heliyon.2020.e03574

Alamiery A, Mahmoudi E, Allami T (2021) Corrosion inhibition of low-carbon steel in hydrochloric acid environment using a Schiff base derived from pyrrole: gravimetric and computational studies. International Journal of Corrosion and Scale Inhibition 10(2):749–765

Ameri E, Jafari H, Rezaeevala M, Vakili MH, Mokhtarian N (2022) Synthesized Schiff base acted as eco-friendly inhibitor for mild steel in 1N H_2SO_4. Chemical Review and Letters 5(2):119–126. https://doi.org/10.22034/crl.2022.328744.1153

Berisha A (2019b) The influence of the grafted aryl groups on the solvation properties of the graphyne and graphdiyne - a MD study. Open Chem 17:703–710. https://doi.org/10.1515/chem-2019-0083

Berisha A (2021) Ab inito exploration of nanocars as potential corrosion inhibitors. Comput Theor Chem 1201:113258. https://doi.org/10.1016/J.COMPTC.2021.113258

Bhardwaj N, Sharma P, Berisha A, Mehmeti V, Dagdag O, Kumar V (2022) Monte Carlo simulation, molecular dynamic simulation, quantum chemical calculation and anti-corrosive behaviour of Citrus limetta pulp waste extract for stainless steel (SS-410) in acidic medium. Mater Chem Phys 284:126052. https://doi.org/10.1016/J.MATCHEMPHYS.2022.126052

Dagdag O, El Harfi A, El Gana L, Safi ZS, Guo L, Berisha A, Verma C, Ebenso EE, Wazzan N, El Gouri M (2021a) Designing of phosphorous based highly functional dendrimeric macromolecular resin as an effective coating material for carbon steel in NaCl: computational and experimental studies. J Appl Polym Sci 138:49673. https://doi.org/10.1002/APP.49673

Daoudi W, El Aatiaoui A, Falil N, Azzouzi M, Berisha A, Olasunkanmi LO, Dagdag O, Ebenso EE, Koudad M, Aouinti A, Loutou M, Oussaid A (2022) Essential oil of dysphania ambrosioides as a green corrosion inhibitor for mild steel in HCl solution. J Mol Liq 363:119839. https://doi.org/10.1016/J.MOLLIQ.2022.119839

Fakhry H, El Faydy M, Benhiba F, Rbaa M, Allaoui M, Warad I, Zarrouk A (2024) Hindering corrosion of carbon steel in the hydrochloric medium by a newly synthesized quinolines: experimental and computational approaches. Journal of Bio-and Tribo-Corrosion. 10(1):11

Furtado LB, Nascimento RC, Henrique FJ, Guimarães MJO, Rocha JC, Ponciano JAC, Seidl PR (2022) Effects of temperature, concentration and synergism on green Schiff bases synthesized from vanillin in applications as corrosion inhibitors for carbon steel in well stimulation. J Petrol Sci Eng 213:110401

Guo L, Zhang ST, Li WP, Hu G, Li X (2014) Experimental and computational studies of two antibacterial drugs as corrosion inhibitors for mild steel in acid media. Mater Corros 65:935–942. https://doi.org/10.1002/maco.201307346

Haldhar R, Prasad D, Bahadur I, Dagdag O, Berisha A (2021) Evaluation of Gloriosa superba seeds extract as corrosion inhibition for low carbon steel in sulfuric acidic medium: a combined experimental and computational studies. J Mol Liq 323:114958. https://doi.org/10.1016/J.MOLLIQ.2020.114958

Inada Y, Orita H (2008) Efficiency of numerical basis sets for predicting the binding energies of hydrogen bonded complexes: evidence of small basis set superposition error compared to Gaussian basis sets. J Comput Chem 29:225–232. https://doi.org/10.1002/jcc.20782

Jafari H, Akbarzade K (2017) Effect of concentration and temperature on carbon steel corrosion inhibition. Journal of Bio-and Tribo-Corrosion 3(1):1–9

Jafari H, Sayin K (2015a) Electrochemical and theoretical studies of adsorption and corrosion inhibition of aniline violet compound on carbon steel in acidic solution. J Taiwan Inst Chem Eng 1(56):181–190

Jafari H, Sayin K (2015b) Electrochemical and theoretical studies of adsorption and corrosion inhibition of aniline violet compound on carbon steel in acidic solution. J Taiwan Inst Chem Eng 56:181–190

Jafari H, Sayin K (2016b) Corrosion inhibition studies of N, N′-bis (4-formylphenol)-1, 2-diaminocyclohexane on steel in 1 HCl solution acid. J Taiwan Inst Chem Eng 1(64):314–324

Jafari H, Danaee I, Eskandari H, RashvandAvei M (2013a) Electrochemical and quantum chemical studies of N, N′-bis(4-hydroxybenzaldehyde)-2,2-dimethylpropandiimine Schiff base as corrosion inhibitor for low carbon steel in HCl solution. Journal of Environmental Science and Health, Part A 48:1628–1641

Jafari H, Danaee I, Eskandari H, RashvandAvei M (2013b) Electrochemical and theoretical studies of adsorption and corrosion inhibition of N, N′-Bis(2-hydroxyethoxyacetophenone)-2,2-dimethyl-1,2-propanediimine on low carbon steel (API 5L grade B) in acidic solution. Ind Eng Chem Res 52:6617–6632

Jafari H, Danaee I, Eskandari H, RashvandAvei M (2014) Combined computational and experimental study on the adsorption and inhibition effects of N_2O_2 Schiff base on the corrosion of API 5L grade B steel in 1 mol/L HCl. J Mater Sci Technol 30:239–252

Jafari H, Ameri E, Rezaeivala M, Berisha A, Halili J (2022b) Anti-corrosion behavior of two N2O4 Schiff-base ligands: experimental and theoretical studies. J Phys Chem Solids 164:110645. https://doi.org/10.1016/J.JPCS.2022.110645

Jafari H, Ameri E, Vakili MH, Berisha A (2024a) Novel silicon-based Schiff-base as corrosion inhibitor for anti-corrosion behavior of API 5L grade B in 1M HCl. Mater Chem Phys 311:128499

Jafari H, Ameri E, Vakili MH, Berisha A (2024b) Effect of OH position on adsorption behavior of Schiff-base derivatives in corrosion inhibition of carbon steel in 1 M HCl. Electrochem Commun 159:107653

Keypour H, Rezaeivala M, Valencia L, Perez-Lourido P (2008) Synthesis and crystal structure of Mn(II) complexes with novel macrocyclic Schiff-base ligands containing piperazine moiety. Polyhedron 27:3172–3176. https://doi.org/10.1016/j.poly.2008.07.012

Keypour H, Rezaeivala M, Valencia L, Perez-Lourido P (2009) Synthesis and characterization of some new Pb (II), Mn (II) and Ag (I) complexes with a pentaaza macrocyclic ligand containing a piperazine moiety. Polyhedron 28:4096–4100. https://doi.org/10.1016/j.poly.2009.09.031

Klamt A (2018) The COSMO and COSMO-RS solvation models. Wiley Interdiscip Rev Comput Mol Sci 8:e1338. https://doi.org/10.1002/wcms.1338

Mardirossian N, Head-Gordon M (2017) Thirty years of density functional theory in computational chemistry: an overview and extensive assessment of 200 density functionals. Mol Phys 115:2315–2372. https://doi.org/10.1080/00268976.2017.1333644

Mohsenifar F, Jafari H, Sayin K (2016) Investigation of thermodynamic parameters for steel corrosion in acidic solution in the presence of N, N′-Bis (phloroacetophenone)-1, 2 propanediamine. Journal of Bio-and Tribo-Corrosion 2(1):1–3

Negm NA, Elkholy YM, Ghuiba FM, Zahran MK, Mahmoud SA, Tawfik SM (2011) Benzothiazol-3-ium cationic Schiff base surfactants: synthesis, surface activity and antimicrobial applications against pathogenic and sulfur reducing bacteria in oil fields. J Dispersion Sci Technol 32(4):512–518

Ouass A, Galai M, Ouakki M, Ech-Chihbi E, Kadiri L, Hsissou R, Essaadaoui Y, Berisha A, Cherkaoui M, Lebkiri A, Rifi EH (2021b) Poly(sodium acrylate) and poly(acrylic acid sodium) as an eco-friendly corrosion inhibitor of mild steel in normal hydrochloric acid: experimental, spectroscopic and theoretical approach. J Appl Electrochem 51:1009–1032. https://doi.org/10.1007/s10800-021-01556-y

Oyeneyin OE, Ojo ND, Ipinloju N, James AC, Agbaffa EB (2022) Investigation of corrosion inhibition potentials of some aminopyridine Schiff bases using density functional theory and Monte Carlo simulation. Chemistry Africa 5(2):319–332

Quraishi MA, Ansari FA, Rawat J (2009) Investigation of piperazine and its derivatives as vapor phase corrosion inhibitors for mild steel. The Open Electrochemistry Journal 1:32–36

Rezaeivala M, Karimi S, Sayin K, B. TÜZÜN (2022) Experimental and theoretical investigation of corrosion inhibition effect of two piperazine-based ligands on carbon steel in acidic media. Colloids and Surfaces A: Physicochemical and Engineering Aspects. 641:128538

Saha SK, Dutta A, Ghosh P, Sukul D, Banerjee P (2015) Adsorption and corrosion inhibition effect of Schiff base molecules on the mild steel surface in 1 M HCl medium: a combined experimental and theoretical approach. Phys Chem Chem Phys 17(8):5679–5690

Zaroual A, Daoui S, El Faydy M, Timoudan N, Chraka A, Zarrok H, Zarrouk, A. (2024) 4-Benzyl-2-(3-(4-fluorophenyl)-2-oxopropyl)-6-phenyl pyridazin-3 (2 H)-one as a carbon steel corrosion inhibitor in an acidic environment: electrochemical, spectroscopic, thermodynamic, and quantum chemical assessments. Journal of Bio-and Tribo-Corrosion 10(3):64

Zhang JT, Bai ZQ, Zhao J, Feng YR, Wang Y (2012) The synthesis and evaluation of N-carbonyl piperazine as a hydrochloric acid corrosion inhibitor for high protective 13Cr steel in an oil field. Pet Sci Technol 30:1851–1861. https://doi.org/10.1080/10916466.2010.512884

Zhang W, Li HJ, Wang M, Wang LJ, Shang F, Wu YC (2018) Halogen-substituted acridines as highly effective corrosion inhibitors for mild steel in acid medium. The Journal of Physical Chemistry C 122(44):25349–25364

Zhao Y, Truhlar DG (2008) The M06 suite of density functionals for main group thermochemistry, thermochemical kinetics, noncovalent interactions, excited states, and transition elements: two new functionals and systematic testing of four M06-class functionals and 12 other functionals. Theor Chem Acc 120:215–241. https://doi.org/10.1007/s00214-007-0310-x

R.L.C. Akkermans, N.A. Spenley, S.H. Robertson, COMPASS III: automated fitting workflows and extension to ionic liquids, Https://Doi.Org/https://doi.org/10.1080/08927022.2020.1808215. 47 (2020) 540–551. https://doi.org/10.1080/08927022.2020.1808215.

B. Ould abdelwedoud, M. Damej, K. Tassaoui, Berisha, H. Tachallait, K. Bougrin, V. Mehmeti, M. Benmessaoud, Inhibition effect of N-propargyl saccharin as corrosion inhibitor of C38 steel in 1M HCl, experimental and theoretical study, J. Mol. Liq. (2022) 118784. https://doi.org/10.1016/J.MOLLIQ.2022.118784.

Benmahammed, I., Douadi, T., Issaadi, S., Al-Noaimi, M., & Chafaa, S. (2019). Heterocyclic Schiff bases as corrosion inhibitors for carbon steel in 1 M HCl solution: hydrodynamic and synergetic effect. Journal of Dispersion Science and Technology. https://www.tandfonline.com/doi/abs/10.1080/01932691.2019.1614038.

A. Berisha, Interactions between the aryldiazonium cations and graphene oxide: a DFT study, J. Chem. 2019 (2019). https://doi.org/10.1155/2019/5126071.

O. Dagdag, R. Hsissou, A. Berisha, H. Erramli, O. Hamed, S. Jodeh, A. El Harfi, Polymeric-based epoxy cured with a polyaminoamide as an anticorrosive coating for aluminum 2024-T3 surface: experimental studies supported by computational modeling, J. Bio- Tribo-Corrosion. 5 (2019). https://doi.org/10.1007/s40735-019-0251-7.

O. Dagdag, R. Hsissou, A. El Harfi, A. Berisha, Z. Safi, C. Verma, E.E.E. Ebenso, M. Ebn Touhami, M. El Gouri, Fabrication of polymer based epoxy resin as effective anti-corrosive coating for steel: computational modeling reinforced experimental studies, Surfaces and Interfaces. 18 (2020) 100454. https://doi.org/10.1016/j.surfin.2020.100454.

O. Dagdag, A. Berisha, V. Mehmeti, R. Haldhar, E. Berdimurodov, O. Hamed, S. Jodeh, H. Lgaz, E.-S.M. Sherif, E.E. Ebenso, Epoxy coating as effective anti-corrosive polymeric material for aluminum alloys: formulation, electrochemical and computational approaches, J. Mol. Liq. (2021) 117886. https://doi.org/10.1016/J.MOLLIQ.2021.117886.

M. Damej, R. Hsissou, A. Berisha, K. Azgaou, M. Sadiku, M. Benmessaoud, N. Labjar, S. El hajjaji, New epoxy resin as a corrosion inhibitor for the protection of carbon steel C38 in 1M HCl. experimental and theoretical studies (DFT, MC, and MD), J. Mol. Struct. 1254 (2022) 132425. https://doi.org/10.1016/J.MOLSTRUC.2022.132425.

M. El Faydy, H. About, I. Warad, Y. Kerroum, A. Berisha, F. Podvorica, F. Bentiss, G. Kaichouh, B. Lakhrissi, A. Zarrouk, Insight into the corrosion inhibition of new bis-quinolin-8-ols derivatives as highly efficient inhibitors for C35E steel in 0.5 M H2SO4, J. Mol. Liq. 342 (2021) 117333. https://doi.org/10.1016/J.MOLLIQ.2021.117333.

Faydy, M. E., Benhiba, F., Alfakeer, M., Al-bonayan, A. M., Timoudan, N., Warad, I., ... & Zarrouk, A. (2023). Corrosion resistance of two newly synthesized 8-quinolinol-benzimidazoles on carbon steel: an experimental and theoretical investigation. Journal of Materials Engineering and Performance. 1–19. https://doi.org/10.1007/s11665-023-08919-w.

R. Ganjoo, S. Sharma, A. Thakur, H. Assad, P. Kumar Sharma, O. Dagdag, A. Berisha, M. Seydou, E.E. Ebenso, A. Kumar, Experimental and theoretical study of sodium cocoyl glycinate as corrosion inhibitor for mild steel in hydrochloric acid medium, J. Mol. Liq. (2022) 119988. https://doi.org/10.1016/J.MOLLIQ.2022.119988.

R. Hsissou, O. Dagdag, S. Abbout, F. Benhiba, M. Berradi, M. El Bouchti, A. Berisha, N. Hajjaji, A. Elharfi, Novel derivative epoxy resin TGETET as a corrosion inhibition of E24 carbon steel in 1.0 M HCl solution. Experimental and computational (DFT and MD simulations) methods, J. Mol. Liq. 284 (2019) 182–192. https://doi.org/10.1016/j.molliq.2019.03.180.

R. Hsissou, B. Benzidia, M. Rehioui, M. Berradi, A. Berisha, M. Assouag, N. Hajjaji, A. Elharfi, Anticorrosive property of hexafunctional epoxy polymer HGTMDAE for E24 carbon steel corrosion in 1.0 M HCl: gravimetric, electrochemical, surface morphology and molecular dynamic simulations, Polym. Bull. 77 3577–3601. https://doi.org/10.1007/s00289-019-02934-5.

Jafari, H., Ameri, E. (2024). Synthesis and evaluation of Schiff base as corrosion inhibitor for carbon steel in 1 M HCl solution. Anti-Corrosion Methods and Materials. https://www.emerald.com/insight/content/doi/10.1108/ACMM-03-2024-2976/full/html?.

H. Jafari, K. Sayin, Sulfur containing compounds as corrosion inhibitors for mild steel in hydrochloric acid solution. Transactions of the Indian Institute of Metals. 69(3), (2016), 805–15. [5] K. Sayin, H. Jafari, Effect of pyridyl on adsorption behavior and corrosion inhibition of aminotriazole. Journal of the Taiwan Institute of Chemical Engineers, 1;68 (2016)431–9.

H. Jafari, K. Akbarzade, I. Danaee, Corrosion inhibition of carbon steel immersed in a 1 M HCl solution using benzothiazole derivatives. Arabian journal of chemistry, 1;12(7)(2019)1387–94.

H. Jafari, M. Rezaeivala, N. Mokhtarian, A. Berisha, E. Ameri, Corrosion inhibition of carbon steel in 0.5 M H2SO4 by new reduced Schiff base ligand, J. Bio- Tribo-Corrosion 2022 83. 8 (2022) 1–13. https://doi.org/10.1007/S40735-022-00679-9.

S.J.H.M.H.M. Jessima, A. Berisha, S.S.S.S. Srikandan, S. Subhashini, Preparation, characterization, and evaluation of corrosion inhibition efficiency of sodium lauryl sulfate modified chitosan for mild steel in the acid pickling process, J. Mol. Liq. 320 (2020) 114382. https://doi.org/10.1016/j.molliq.2020.114382.

F. El Kalai, T. Chelfi, N. Benchat, B. Hacht, M. Bouklah, A. Elaatiaoui, S. Daoui, M. Allali, T. Ben Hadda, F. Almalki, New organic extractant based on pyridazinone scaffold compounds: liquid-liquid extraction study and DFT calculations, J. Mol. Struct. 1191 (2019) 24–31. https://doi.org/10.1016/j.molstruc.2019.04.033.

H. Keypour, N. Rahpeyma, M. Rezaeivala, P. Arzhangi, M. Bayat, L. Valencia, Y. Elerman, O. Büyükgüngör, Synthesis and structural characterization of a new Schiff base macrocyclic ligand containing a piperazine head unit and its metal complexes. Crystal structure of the Co (II) complex. Polyhedron 51 (2013) 117–122. https://doi.org/10.1016/j.poly.2012.12.020.

A. Klamt, COSMO-RS: from quantum chemistry to fluid phase thermodynamics and drug design, Elsevier, 2005.

M. Ben Hadj Ayed, T. Osmani, N. Issaoui, A. Berisha, B. Oujia, H. Ghalla, Structures and relative stabilities of Na+Nen (n = 1–16) clusters via pairwise and DFT calculations, Theor. Chem. Acc. 138 (2019) 84. https://doi.org/10.1007/s00214-019-2476-4.

V. Mehmeti, Nystatin drug as an effective corrosion inhibitor for mild steel in acidic media– an experimental and theoretical study, Corros. Sci. Technol. 21 (2022) 21–31. https://doi.org/10.14773/CST.2022.21.1.21.

A. Molhi, R. Hsissou, M. Damej, A. Berisha, M. Bamaarouf, M. Seydou, M. Benmessaoud, S. El Hajjaji, Performance of two epoxy compounds against corrosion of C38 steel in 1 M HCl: electrochemical, thermodynamic and theoretical assessment, Int. J. Corros. Scale Inhib. 10 (2021) 812–837. https://doi.org/10.17675/2305-6894-2021-10-2-21.

A. Molhi, R. Hsissou, M. Damej, A. Berisha, V. Thaçi, A. Belafhaili, M. Benmessaoud, N. Labjar, S. El Hajjaji, Contribution to the corrosion inhibition of c38 steel in 1 m hydrochloric acid medium by a new epoxy resin pgeppp, Int. J. Corros. Scale Inhib. 10 (2021) 399–418. https://doi.org/10.17675/2305-6894-2021-10-1-23.

A. Ouass, M. Galai, M. Ouakki, E. Ech-Chihbi, L. Kadiri, R. Hsissou, Y. Essaadaoui, A. Berisha, M. Cherkaoui, A. Lebkiri, E.H. Rifi, Poly(sodium acrylate) and poly(acrylic acid sodium) as an eco-friendly corrosion inhibitor of mild steel in normal hydrochloric acid: experimental, spectroscopic and theoretical approach, J. Appl. Electrochem. 2021 517. 51 (2021) 1009–1032. https://doi.org/10.1007/S10800-021-01556-Y.

B. Ould Abdelwedoud, M. Damej, K. Tassaoui, A. Berisha, H. Tachallait, K. Bougrin, V. Mehmeti, M. Benmessaoud, Inhibition effect of N-propargyl saccharin as corrosion inhibitor of C38 steel in 1 M HCl, experimental and theoretical study, J. Mol. Liq. 354 (2022) 118784. https://doi.org/10.1016/J.MOLLIQ.2022.118784.

A. Rahimi, A. Farhadian, A. Berisha, A. Shaabani, M.A. Varfolomeev, V. Mehmeti, X. Zhong, S. Yousefzadeh, R. Djimasbe, Novel sucrose derivative as a thermally stable inhibitor for mild steel corrosion in 15% HCl medium: an experimental and computational study, Chem. Eng. J. (2022) 136938. https://doi.org/10.1016/J.CEJ.2022.136938.

Timoudan, N., Faydy, M. E., Titi, A., Warad, I., Benhiba, F., Alsulmi, A., ... & Zarrouk, A. (2024). Enhanced corrosion resistance of carbon steel in an aggressive environment by a recently developed pyrazole derivative: electrochemical, SEM/XPS/AFM, and theoretical investigation. Journal of Solid State Electrochemistry. 1–24. https://link.springer.com/article/10.1007/s10008-024-05846-1.

Publisher's Note